Molecular Therapy
Nucleic Acids
Original Article

Unique quinoline orientations shape the modified aptamer to sclerostin for enhanced binding affinity and bone anabolic potential

Amu Gubu,[1,2,7] Yuan Ma,[1,2,3,7] Sifan Yu,[1,4,5,7] Huarui Zhang,[1,4,7] Zefeng Chen,[1,2,3,7] Shuaijian Ni,[1,7] Razack Abdullah,[1,2,6] Huan Xiao,[1,4] Yihao Zhang,[1,4] Hong Dai,[1] Hang Luo,[1,4] Yuanyuan Yu,[1,2] Luyao Wang,[1,2] Hewen Jiang,[1,4] Ning Zhang,[1,4] Yuan Tian,[2,6] Haitian Li,[2,6] Aiping Lu,[1] Baoting Zhang,[4] and Ge Zhang[1,2]

[1]Guangdong-Hong Kong-Macao Greater Bay Area International Research Platform for Aptamer-based Translational Medicine and Drug Discovery, Hong Kong SAR 999077, China; [2]Law Sau Fai Institute for Advancing Translational Medicine in Bone & Joint Diseases, School of Chinese Medicine, Hong Kong Baptist University, Hong Kong SAR 999077, China; [3]Increasepharm & Hong Kong Baptist University Joint Centre for Nucleic Acid Drug Discovery, Hong Kong Science Park, New Territories, Hong Kong, China; [4]School of Chinese Medicine, Faculty of Medicine, The Chinese University of Hong Kong, Hong Kong SAR 999077, China; [5]Shenzhen Research Institute, The Chinese University of Hong Kong, School of Chinese Medicine, The Chinese University of Hong Kong, Shen Zhen 518063, China; [6]Institute of Integrated Bioinfomedicine and Translational Science, School of Chinese Medicine, Hong Kong Baptist University, Kowloon Tsai, Hong Kong 999077, China

Osteogenesis imperfecta (OI) is a rare genetic disease characterized by bone fragility and bone formation. Sclerostin could negatively regulate bone formation by antagonizing the Wnt signal pathway, whereas it imposes severe cardiac ischemic events in clinic. Our team has screened an aptamer that could promote bone anabolic potential without cardiovascular risk. However, the affinity of the aptamer is lower and needs to be improved. In the study, hydrophobic quinoline molecule with unique orientations (seven subtypes) were incorporated into key sites of a bone anabolic aptamer against sclerostin to form a modified aptamer library. Among all the quinoline modifications, 5-quinoline modification could shape the molecular recognition of modified aptamers to sclerostin to facilitate enhancing its binding to sclerostin toward the highest affinity by interacting with newly participated binding sites in sclerostin. Further, 5-quinoline modification could facilitate the modified aptamer attenuating the suppressed effect of the transfected sclerostin on both Wnt signaling and bone formation marker expression levels *in vitro*, promoting bone anabolism in OI mice (*Col1a2*$^{+/G610C}$). The proposed quinoline-oriented modification strategy could shape the molecular recognition of modified aptamers to proteins to facilitate enhancing its binding affinity and therapeutic potency.

INTRODUCTION

Nucleic acid aptamers are short fragments of DNA or RNA that can recognize and bind to target molecules. Aptamers are usually selected from pools of randomly synthesized oligodeoxynucleotides or oligonucleotides using Systematic Evolution of Ligands by Exponential Enrichment (SELEX) technology.[1] In comparison with antibodies, aptamers are increasingly emerging as a powerful alternative due to their ease of synthesis, low immunogenicity, high stability, and broad range of target recognition.[2] Although researchers have developed thousands of aptamers against various targets in basic research,[3] only two aptamers (pegaptanib against vascular endothelial growth factor,[4] and izervay against C5) have been approved by the U.S. Food and Drug Administration. Many nucleic acid aptamers that entered in clinical trials were discontinued for their limited therapeutic efficacy. It is known that the binding ability of the aptamer drug candidates to the targets largely contributes to their relevant pharmacodynamics. For example, AS1411 was discontinued due to its minimal efficacy shown in phase II clinical trials.[5] For developing the next generation of AS1411, Fan et al.[6] synthesized a chemically modified AS1411 with 31.5-fold affinity enhancement significantly suppressed MCF-7 Xenografts. Similarly, an E-selectin antagonistic thioaptamer exhibited a 1,000-fold lower median inhibition concentration to the naturally unmodified ligand, which could be explained by a more than 10,000-fold affinity enhancement.[7] Thus, the development of a high-affinity modification strategy can help to address the druggability bottleneck of aptamers.

It is critical for aptamers to tightly interact with the target ligand (usually protein) to obtain high binding affinity. Structurally, aptamers

Received 6 November 2023; accepted 9 February 2024;
https://doi.org/10.1016/j.omtn.2024.102146.

[7]These authors contributed equally

Correspondence: Yuan Ma, Guangdong-Hong Kong-Macao Greater Bay Area International Research Platform for Aptamer-based Translational Medicine and Drug Discovery, Hong Kong SAR 999077, China.
E-mail: mayuan@hkbu.edu.hk
Correspondence: Baoting Zhang, School of Chinese Medicine, Faculty of Medicine, The Chinese University of Hong Kong, Hong Kong SAR 999077, China.
E-mail: zhangbaoting@cuhk.edu.hk
Correspondence: Ge Zhang, Guangdong-Hong Kong-Macao Greater Bay Area International Research Platform for Aptamer-based Translational Medicine and Drug Discovery, Hong Kong SAR 999077, China.
E-mail: zhangge@hkbu.edu.hk

could form different shapes to interact with the ligands through non-covalent bonding, including hydrogen bonding, π-π stacking, London dispersion forces, ion-ion interactions, and dipole-dipole interactions.[8] Hydrophobic groups have widely emerged to enhance the binding affinity of the modified aptamers to target proteins.[9] For instance, Davies et al.[10] and Gawande et al.[11] expanded DNA chemistry by endowing aptamers with hydrophobic amino acid-like side chains (benzyl, isobutyl, naphthyl, indoyl, pyridyl, pyrrolyl, etc) through modified-SELEX (mod-SELEX). These modified aptamers (named SOMAmers) embodied slow off-rate to proteins by enlarging the hydrophobic interaction shape,[10,11] held promising prospects because of comparable binding affinities to antibodies.[12] However, the diversity of the above mod-SELEX modifications was restricted by the DNA polymerase. Post-SELEX modification strategies preserved simplicity, flexibility, and reduced selection bias compared with mod-SELEX modification strategies. Smirnov et al.[13] attempted to increase the contact areas of aptamer to thrombin by adding two hydrophobic group through post-SELEX. Regrettably, the selected modification types and modification sites were not well designed, leading to moderate affinity enhancement (2-fold).[13] Thus, it is necessary to establish an efficient hydrophobic modification strategy to enhance the affinity of the aptamer in drug design.

Osteogenesis imperfecta (OI) is an inherited bone disorder, causing low bone mass and abnormal architecture.[14] Mechanistically, the circulating protein sclerostin could bind to low-density lipoprotein receptor-related protein 5 and 6 (*Lrp5/6*) and antagonize the Wnt signaling pathway, thereby negatively regulating bone formation. Genetically, mutation on *Lrp5* could increase bone mass and enhance bone strength in OI mice (*Col1a2*$^{+/G610C}$ mice). Pharmacologically, sclerostin antibody treatment could also increase bone mass and enhance bone strength in OI mice.[15] However, the marketed sclerostin antibody (romosozumab) increases the risk of cardiovascular outcomes.[16] Our previously screened sclerostin aptamer (Aptscl56) was proved to exert bone anabolic potential without increased cardiovascular concerns.[17,18] Thus, it is necessary to enhance the binding affinity of Aptscl56 to sclerostin using an efficient hydrophobic modification strategy for clinical translation.

In the study, hydrophobic quinoline molecule was predicted to tightly bind to sclerostin. Meanwhile, a total of 22 sites in Aptscl56 were identified as key sites to play vital roles in the interactions to sclerostin. Therefore, the different quinoline derivates (seven subtypes) were incorporated into the key sites in the aptamer to form a modified aptamer library. Then, the quinoline modified aptamer with the highest binding affinity was identified from the library. Subsequently, the bone anabolic potential of the quinoline modified aptamer was evaluated both *in vitro* and *in vivo*. Structurally, the difference in binding sites of sclerostin to aptamer with and without quinoline modification was studied. Mechanistically, the roles of the newly participated binding sites in the binding ability with the quinoline modified aptamer were studied. Moreover, the roles of the newly participated binding sites in the re-activation effect of the quinoline modified aptamer on the suppressed Wnt signaling were also examined.

RESULTS

In total, 22 key sites in Aptscl56 were identified using point mutation with either C3 spacer or dspacer tetrahydrofuran

The key sites of Aptscl56, against sclerostin, was first identified to facilitate quinolyl modification deliberately. Using a flexible linker (C3 spacer) (Figure S1A) that lacks both the sugar ring and the base, but maintains the same number of carbons between phosphates, point mutations were performed to examine the roles of the sites in the aptamer interacting with sclerostin (Table S1). Through an enzyme-linked oligonucleotides assay (ELONA) that utilizes horseradish peroxidase (HRP) for signaling production, the sites 3–6, 8, 15, 29, and 32–40 in Aptscl56 were identified, which played important roles in the interactions of the aptamer to sclerostin (Figure S1B).

The C3 spacer is too flexible compared with natural nucleoside spacer, which might lead to undesired structural variations. Therefore, a dspacer tetrahydrofuran (THF) (Figure S1C) that only lacks the nucleoside base and maintains the sugar ring compared with C3 spacer was involved to examine the roles of the sites of Aptscl56 in interacting with sclerostin (Table S2). Through the same screening procedure as C3 spacer, the binding ability altered significantly with dspacer THF substitution in site 1–5, 11, 13, 15, and 30–40, which indicated that those sites played important roles in the interactions of the aptamer to sclerostin (Figure S1D).

Collectively, the above data demonstrated that the mutation of the particular sites (1–6, 8, 11, 13, 15, and 29–40) in the aptamer significantly altered the binding ability of the aptamer to sclerostin, indicating that those particular sites (22 in total) were the key sites in the aptamer interacting with sclerostin.

5-Quinoline modification could facilitate enhancing the binding ability of the modified aptamers to sclerostin toward the highest binding affinity

It was reported that hydrophobic modifications could strengthen the interactions of the modified nucleic acids to cognate targets due to the elevated van der Waals' force.[19,20] To structurally understand the role of listed hydrophobic molecules interacting with sclerostin, molecular dynamics simulation was performed to predict the binding sites of sclerostin. Site 60 in sclerostin was predicted to form one Pi-Pi stacking bond with quinoline (5.0 Å) (Figure S2). Site 116 in sclerostin was predicted to form two Pi cation bonds with quinoline (4.3 Å, 5.0 Å) (Figure S2). Among the listed hydrophobic molecules, hydrophobic quinoline molecule (n1) was predicted to tightly interact with sclerostin with the smallest Gibbs free energy for binding (Table S3). To strengthen the interactions of the modified aptamer to sclerostin, a series of quinoline derivates (2-quinoline to 8-quinoline) (Figure 1A) modification with high hydrophobicity were designed and synthesized. These quinoline derivates (seven in total) have the same structure, but differential orientation. To compare the difference in the binding ability of the modified aptamer to sclerostin protein, 154 aptamers (7 × 22) modified with the above synthesized 7 quinoline derivates in the above identified 22 binding sites were obtained by

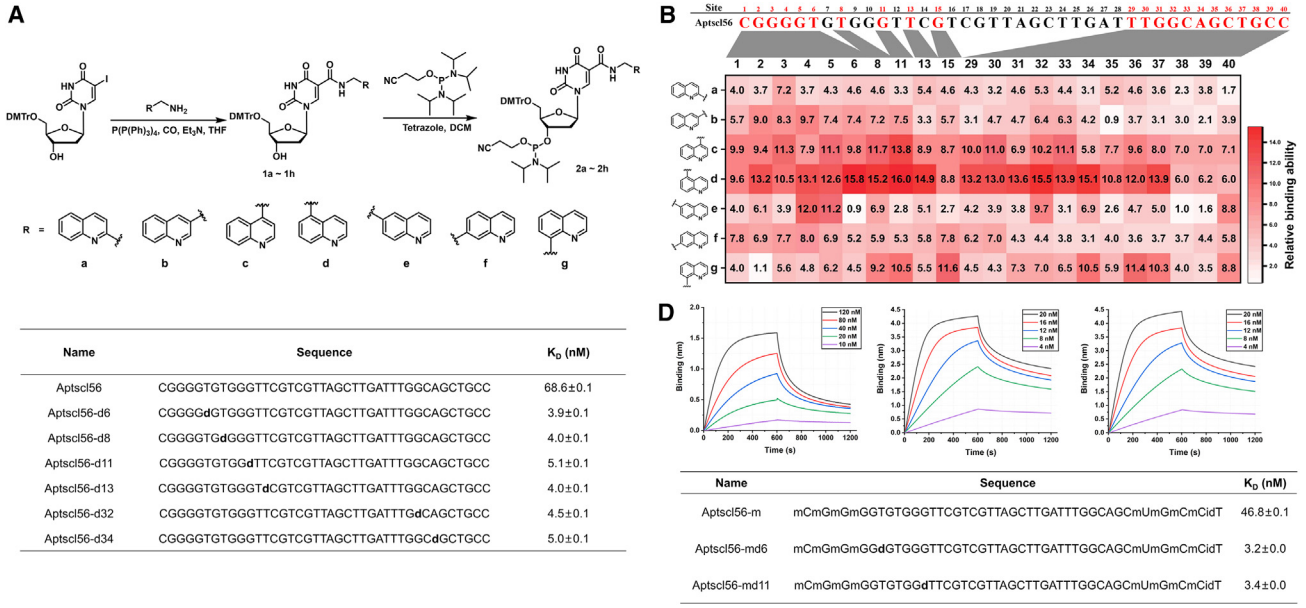

Name	Sequence	K_D (nM)
Aptscl56	CGGGGTGTGGGTTCGTCGTTAGCTTGATTTGGCAGCTGCC	68.6±0.1
Aptscl56-d6	CGGGG**d**GTGGGTTCGTCGTTAGCTTGATTTGGCAGCTGCC	3.9±0.1
Aptscl56-d8	CGGGGTG**d**GGGTTCGTCGTTAGCTTGATTTGGCAGCTGCC	4.0±0.1
Aptscl56-d11	CGGGGTGTGG**d**TTCGTCGTTAGCTTGATTTGGCAGCTGCC	5.1±0.1
Aptscl56-d13	CGGGGTGTGGGT**d**CGTCGTTAGCTTGATTTGGCAGCTGCC	4.0±0.1
Aptscl56-d32	CGGGGTGTGGGTTCGTCGTTAGCTTGATTTG**d**CAGCTGCC	4.5±0.1
Aptscl56-d34	CGGGGTGTGGGTTCGTCGTTAGCTTGATTTGGC**d**GCTGCC	5.0±0.1

Name	Sequence	K_D (nM)
Aptscl56-m	mCmGmGmGGTGTGGGTTCGTCGTTAGCTTGATTTGGCAGCmUmGmCmCidT	46.8±0.1
Aptscl56-md6	mCmGmGmGG**d**GTGGGTTCGTCGTTAGCTTGATTTGGCAGCmUmGmCmCidT	3.2±0.0
Aptscl56-md11	mCmGmGmGGTGTGG**d**TTCGTCGTTAGCTTGATTTGGCAGCmUmGmCmCidT	3.4±0.0

Figure 1. 5-Quinoline modification could facilitate enhancing the binding ability of the modified aptamers to sclerostin towards the highest binding affinity
(A) Seven quinoline derivates with high hydrophobicity were designed and synthesized. **a-g** represented 2-quinoline, 3-quinoline, 4-quinoline, 5-quinoline, 6-quinoline, 7-quinoline, 8-quinoline, respectively. (B) ELONA data of 7 quinoline derivates at 22 key sites. For each sequence, only one site and one substitution were allowed. Totally, binding ability of 154 modified aptamers were evaluated. The binding ability of each sequence was normalized to naturally unmodified Aptscl56. n ≥ 3 each group. (C) The measured K_D values by BLI of the selected Aptscl56-d6, Aptscl56-d8, Aptscl56-d11, Aptscl56-d13, Aptscl56-d32, and Aptscl56-d34 against sclerostin, respectively. (D) Binding affinity data of Aptscl56 modified with both 5-qionoline and enzyme-resistant modifications against sclerostin, including Aptscl56-m, Aptscl56-md6, and Aptscl56-md11. The upper are the BLI curves consisting of association and disassociation processes. The lower are the measured K_D values of Aptscl56-m, Aptscl56-md6, and Aptscl56-md11, respectively. m, methoxy modified nucleoside.

using standard solid-phase DNA synthesis. For each sequence, only one site and one substitution were allowed (Tables S4 and S5). Standardized by naturally unmodified Aptscl56, the relative binding ability of all the modified aptamers against sclerostin was evaluated by ELONA. The *in vitro* data demonstrated that the quinoline modification could generally facilitate enhancing the binding ability of the modified aptamer to sclerostin. Among the seven quinoline modifications, 5-quinoline modification could remarkably facilitate enhancing the binding ability of the modified aptamer to sclerostin for 6–16 times (Figure 1B). Over 14-fold enhancement of binding ability was obtained by 5-quinoline modification at the 6th (Aptscl56-d6), 8th (Aptscl56-d8), 11th (Aptscl56-d11), 13th (Aptscl56-d13), 32nd (Aptscl56-d32), and 34th (Aptscl56-d34) sites. So, 5-quinoline showed much stronger ability in enhancing binding affinity than benzyl modification, which was a commonly used modification in SOMAmers (positive control) (Figure S3).

Further, 5-quinoline-modified Aptscl56, including Aptscl56-d6, Aptscl56-d8, Aptscl56-d11, Aptscl56-d13, Aptscl56-d32, and Aptscl56-d34, were selected to precisely evaluate their binding affinity to sclerostin using biolayer interferometry (BLI). As shown in Figures S4 and 1C, more than 15-fold of the binding affinity was enhanced (from 68.6 nM to 3.86 nM for the dissociation constant [K_D] value), which completely dropped by an order of magnitude with single 5-quinoline modification. Next, we synthesized different combinations of multiple 5-quinoline-modified Aptscl56 at the 6th, 11th, and 32nd sites, including Aptscl56-d6d11, Aptscl56-d6d32, and Aptscl56-d11d32. Unexpectedly, these multiple modifications could not improve the binding affinity of Aptscl56 to sclerostin compared with single 5-quinoline modification. The BLI data revealed that these aptamers with 5-quinoline modified at multiple sites had stronger binding affinities than naturally unmodified Aptscl56, but presented a weaker binding affinity than Aptscl56 with a 5-quinoline modification at a single site (Figure S5). It may be due to the influence of different modifications on the three-dimensional structure. As predicted by molecular docking in Tables S8 and S9, the binding energy with a single quinoline modification was lower than that of multiple modification, while the sites and bonds for binding differ from each other.

To meet the functional requirement by pharmacological studies *in vitro* and *in vivo*, enzyme-resistant modifications were needed for the aptamers against sclerostin. Using our established ribonuclease-resistant modification strategy, four 2′-O-methylation (2′-OMe) groups modifications were incorporated into Aptscl56 at both 5′-terminal and 3′-terminal, as well as an inverted deoxythymidine (idT) coupled to the 3′-terminal. The serum tolerance assay indicated that the 2′-OMe and idT modifications indeed improved the viability of aptamer in serum, while the quinoline modification did little to the viability (Figure S6). Then, the binding affinity of these modified aptamers to sclerostin were evaluated. Interestingly, the binding affinity was moderately increased after

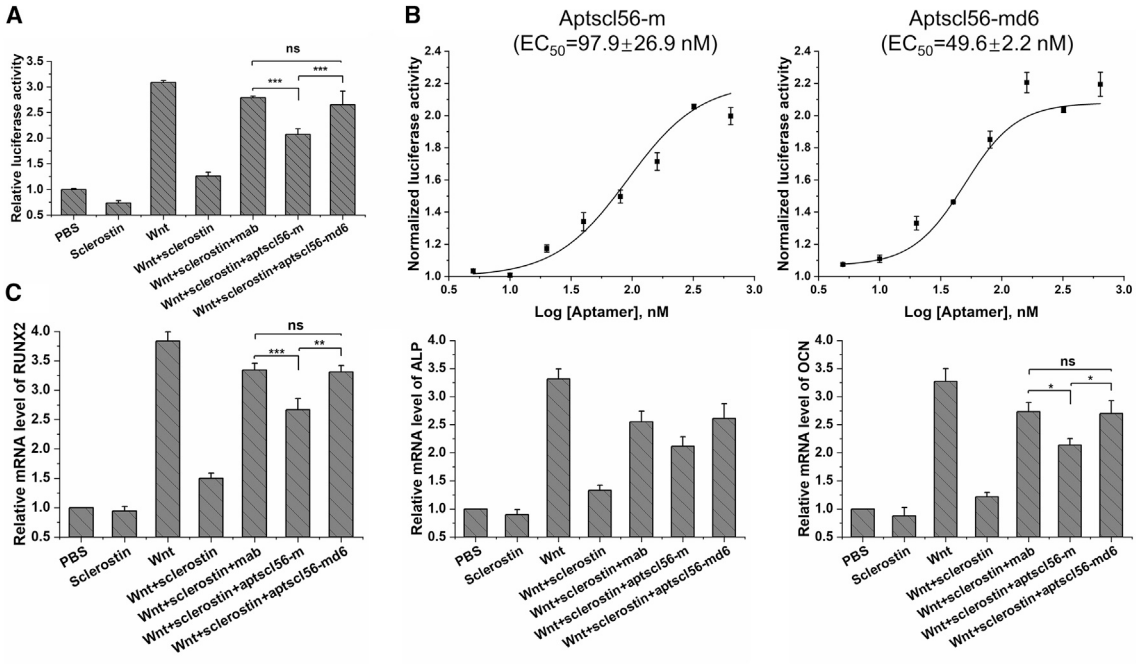

Figure 2. 5-Quinoline modification could remarkably facilitate the modified aptamer attenuating the suppressed effect of the transfected sclerostin on Wnt signaling and promoting bone formation marker expression levels *in vitro*

(A) The effect of sclerostin antibody Romosozumab, Aptscl56-m, and Aptscl56-md6, respectively, on the suppressed Wnt signaling induced by the transfected sclerostin *in vitro*. (B) EC_{50} measurements of Aptscl56-m and Aptscl56-md6, respectively. n = 3 each group. (C) The effect of sclerostin antibody romosozumab (mab), Aptscl56-m, and Aptscl56-md6, respectively, on the down-regulated mRNA expression levels of bone formation markers, including *Runx2*, *Alp*, and *Ocn*, induced by the transfected sclerostin *in vitro*. Data were normalized by parameters in the PBS groups and expressed as mean ± SD. One-way ANOVA with Tukey test was used to determine the inter-group differences, respectively. n = 3 each group. *$p < 0.05$, **$p < 0.01$, ***$p < 0.001$. Note: PBS represented groups treated with1× PBS, which had the same volume with other groups. Sclerostin represented groups transfected with sclerostin plasmid. Wnt represented groups transfected with Wnt-1 plasmid.

both 2′-OMe and idT modifications in Aptscl56-md6 (Aptscl56-d6 with ribonuclease-resistant modification) and Aptscl56-md11 (Aptscl56-md11 with ribonuclease-resistant modification), respectively (Figure 1D).

5-Quinoline modification could facilitate the modified aptamer attenuating the suppressed effect of the transfected sclerostin on both Wnt signaling and bone formation marker expression levels *in vitro*

To precisely evaluate the effect of the 5-quinoline-modified aptamer on the suppressed Wnt signaling induced by the transfected sclerostin, a TCF/LEF luciferase reporter HEK293 cell line was utilized. This cell line is stably transfected HEK293 cell line, which expresses the Renilla luciferase reporter gene under the control of the TCF/LEF response element. It is designed to monitor the transcriptional activity of TCF/LEF and can be used for studying Wnt signaling pathways, as well as screening of activators or inhibitors that affect the TCF/LEF transcriptional activity.[21,22] In this study, the cells were firstly co-transfected with a Wnt-1 plasmid and a sclerostin plasmid to construct a model in which Wnt signaling induced by Wnt-1 was greatly suppressed by sclerostin. After the cells were treated with sclerostin inhibitors, the Wnt signaling would be reactivated. As expected, the data demonstrated that the Wnt-1 induced luciferase signaling was greatly suppressed by sclerostin, confirming the suppressed effect of the transfected sclerostin on Wnt signaling. Surprisingly, when treated with Aptscl56-md6, the luciferase signaling recovered to 86% of that induced by Wnt-1, which was almost the same level of that treated with sclerostin antibody romosozumab and nearly 19% higher than that treated with by Aptscl56-m (Figure 2A). Consequently, the median effective concentration (EC_{50}) measurement revealed that the EC_{50} of Aptscl56-m was 97.9 nM, while that of Aptscl56-md6 was 49.6 nM ($p < 0.05$) (Figure 2B). Further, we compared the effect of different quinoline subtypes modified Aptscl56 at site 6, including 2-quinoline (Aptscl56-ma6), 3-quinoline (Aptscl56-mb6), 4-quinoline (Aptscl56-mc6), 5-quinoline (Aptscl56-md6), 6-quinoline (Aptscl56-me6), 7-quinoline (Aptscl56-mf6), and 8-quinoline (Aptscl56-mg6), as well as a benzene modification (mB6) as a control (Table S6), on reactivating the suppressed Wnt signaling induced by the transfected sclerostin. Among them, 5-quinoline demonstrated the best capability (Figure S7).

Functionally, MC3T3-E1 cell line, a preosteoblast-like cell line, was utilized to evaluate the effect of 5-quinoline modification on the down-regulated mRNA expression levels of the bone formation markers (*Runx2*; consequently, the lower K_D value of multiple, *Ocn*) induced by transfected sclerostin. The cells were co-transfected

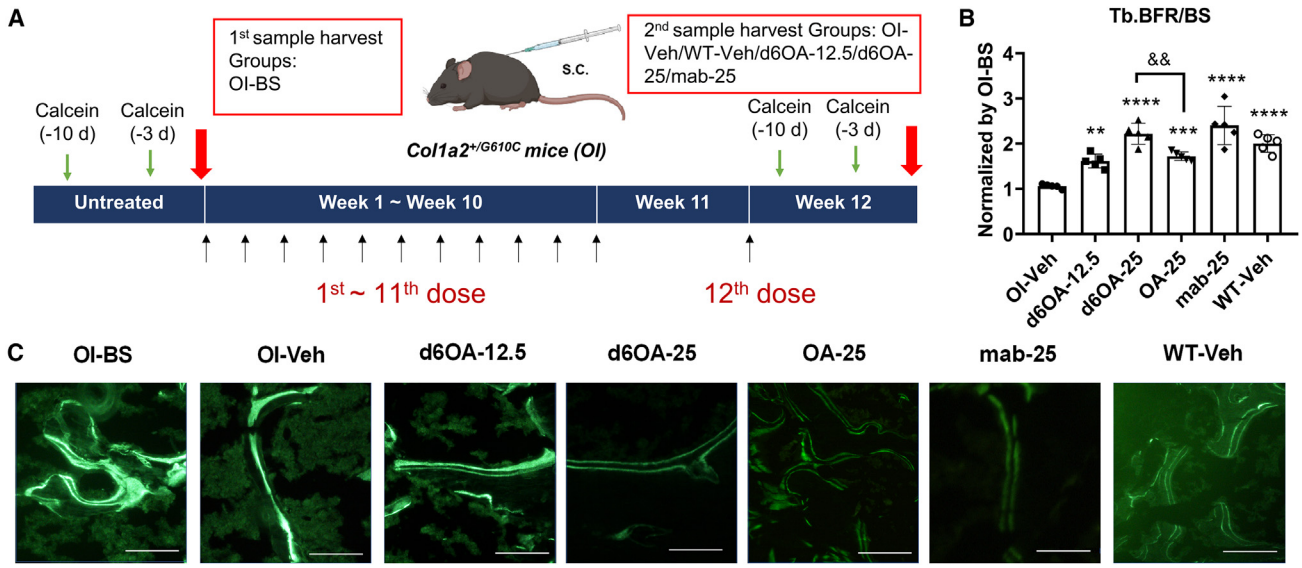

Figure 3. 5-Quinoline could facilitate the modified Aptscl56 promoting the bone formation of the distal femur in *Col1a2*$^{+/G610C}$ OI mice

(A) The schematic diagram for the *in vivo* study. (B) Analysis of dynamic bone histomorphometric parameters of Tb.BFR/BS at the proximal tibia. Data were expressed as mean ± SD followed by one-way ANOVA with Tukey's post hoc test. ****p < 0.0001 versus OI-Veh; $^{\&\&}$p < 0.0001 versus OA-25. n = 5 each group. (C) One group representative fluorescent micrographs of the trabecular bone sections showing bone formation at the proximal tibia visualized by calcein green labels. Scale bars, 0.1 mm n = 5 each group (the other four group images in Figure S8). Note: OI-BS, OI-Baseline; OI-Veh, OI-Vehicle; d6OA-12.5, Aptscl56-md6OA (12.5 mg/kg); d6OA-25, Aptscl56-md6OA (25 mg/kg); OA-25, Aptscl56-mOA (25 mg/kg); mab-25, sclerostin antibody (25 mg/kg); WT-Veh, WT-Vehicle.

with Wnt-1 plasmid and human sclerostin plasmid, followed by treatment with sclerostin antibody romosozumab, Aptscl56-m, and Aptscl56-md6, respectively. Then, the mRNA expression level was quantified by real-time qPCR. Consistent with luciferase assay, when treated with Aptscl56-md6, the relative mRNA expression level recovered to more than 75% of that induced by Wnt-1 (86% for *Runx2*, 79% for *Alp*, and 82% for *Ocn*, respectively), which was the same level of that treated with sclerostin antibody romosozumab (87% for *Runx2*, 77% for *Alp*, and 84% for *Ocn*, respectively) and 15%–19% higher than that treated with Aptscl56-m (19% for *Runx2*, 15% for *Alp*, and 17% for *Ocn*, respectively) (Figure 2C).

Collectively, it indicated that 5-quinoline modification could facilitate the modified aptamer attenuating the suppressed effect of the transfected sclerostin on Wnt signaling and bone formation marker expression levels *in vitro*.

5-Quinoline modification could facilitate the modified aptamer, increasing bone mass, improving bone architecture, promoting bone formation, and enhancing bone mechanical properties in osteogenesis imperfect mice (*Col1a2*$^{+/G610C}$)

To evaluate the effect of 5-quinoline modification on facilitating the modified aptamer promoting bone anabolism in OI mice, Bone histomorphometric analysis and micro-computed tomography (micro-CT) analysis were used to measure the trabecular bone at the metaphysis of both distal femur and proximal tibia, the cortical bone at the femoral mid-shaft in *Col1a2*$^{+/G610C}$ mice. Six- to eight-week-old OI mice were subcutaneously administrated (once per week, 12 weeks) with PBS (OI-Veh), Aptscl56-md6OA 12.5 mg/kg (d6OA-12.5), Aptscl56-md6OA 25 mg/kg (d6OA-25), Aptscl56-mOA 25 mg/kg (OA-25) and sclerostin antibody 25 mg/kg (mab-25). The wild-type mice were subcutaneously administrated (once per week, 12 weeks) with PBS (WT-Veh). The *Col1a2* $^{+/G610C}$ mice were sacrificed before the treatment as OI-Baseline (OI-BS) (Figure 3A). After normalized by the parameters in OI baseline groups, we compared the difference in the trabecular bone formation rate (Tb.BFR/BS) parameters among the group indicated (Figure 3B and 3C, S8). The amount of new bone formed in unit time per unit of bone surface in d6OA-25 group and mab-25 group were higher than those in d6OA-12.5 and OA-25 group. It was found that d6OA-25 group had higher Tb.BFR/BS (+24%, P<0.0001 for diatal femur) over OA-25 group, indicating 5-quinoline facilitated the modified aptamer promoting bone formation. Cortical (Ct). periosteal perimeter and Ct. bone strength index for evaluating the cortical bone microarchitecture was calculated; trabecular volumetric bone mineral density (Tb.vBMD) for evaluating trabecular bone mass was calculated, as well as trabecular connectivity density (Tb.Conn.D) and trabecular number (Tb.N) for evaluating trabecular microarchitecture integrity. For the distal femur, the micro-CT data showed that d6OA-25 group had significantly higher Tb.Conn.D (+49%, P<0.05), Tb.vBMD (+40%, P<0.05) and Tb.N (+33%, P<0.05) in comparison to the OA-25 group. The above parameters were restored to the wild-type levels (WT-Veh) after 12 weeks of d6-25 treatment in *Col1a2* $^{+/G610C}$ mice. There were no significant differences in the above parameters between d6OA group and mab group

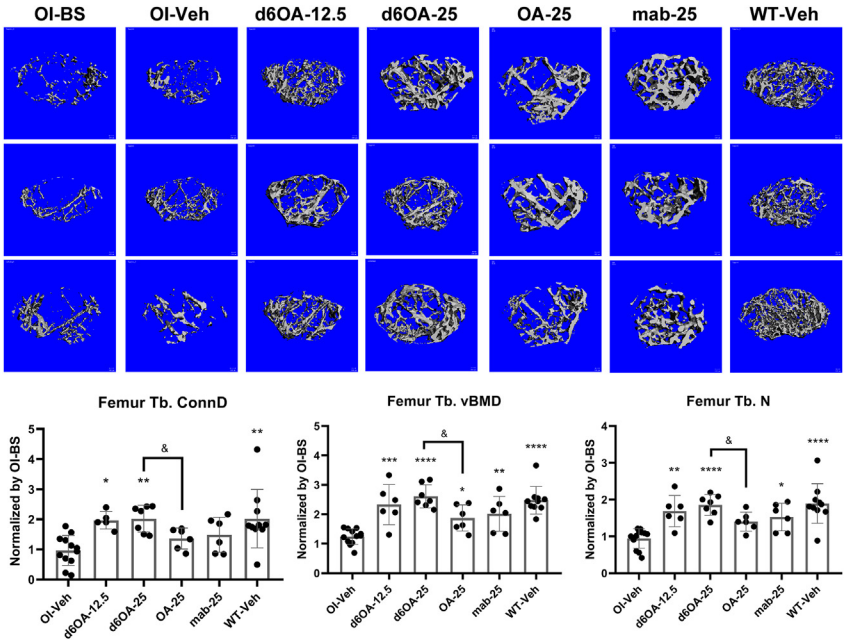

Figure 4. 5-Quinoline could facilitate the modified Aptscl56 increasing trabecular bone mass and improving trabecular microarchitecture of distal femur in *Col1a2*$^{+/G610C}$ OI mice

Representative images showing three-dimensional trabecular architecture by micro-CT reconstruction at the distal femur. Scale bars, 1 mm (top). Bar graphs of the structural parameters of Tb. conn.D, Tb; vBMD, Tb. N from *ex vivo* micro-CT examination at trabecular bone of the distal femur (the below panel). n ≥ 6 each group. Note: Tb. conn.D, trabecular connect density; Tb. vBMD, trabecular volumetric mineral density; Tb. N, trabecular number OI-BS, OI-Baseline; OI-Veh, OI-Vehicle; d6OA-12.5, Aptscl56-md6OA (12.5 mg/kg); d6OA-25, Aptscl56-md6OA (25 mg/kg); OA-25, Aptscl56-mOA (25 mg/kg); mab-25, sclerostin antibody (25 mg/kg); WT-Veh, WT-Vehicle. Data were normalized by the parameters in the OI baseline groups and expressed as mean ± SD followed by one-way ANOVA with Tukey's post hoc test. *p < 0.05; **p < 0.01; ***p < 0.001; ****p < 0.0001 versus OI-Veh; $^{\&}$p < 0.05 versus OA-25.

(P>0.05) (Figure 4). Consistently, for the proximal tibia, the micro-CT data showed that d6OA-25 group had significantly higher Tb.Conn.D (+48%, P<0.05) and Tb.vBMD (+118%, P<0.0001) in comparison to the OA-25 group. There were no significant differences in the above parameters between d6OA group and mab group (P>0.05) (Figure S9). It was found that d6OA-25 group had higher Ct. periosteal perimeter (+11.3%, P<0.01 for femoral mid-shaft), and Ct. bone strength index (+38%, P<0.05 for femoral mid-shaft) (Figure S10) over OA-25 group, indicating 5-quinoline facilitated the modified aptamer improving cortical bone microarchitecture.

To evaluate the effect of 5-quinoline modification on facilitating the modified aptamer enhancing bone mechanical properties, the compression test was used for measurement of the 5th lumbar vertebrae. The compression test is a mechanical evaluation that investigates how a material or product reacts when subjected to a range of forces, including pushing, compressing, squashing, crushing, and flattening of the test specimen. Similar in essence to tensile and bend tests, compression testing is a fundamental mechanical examination. Its primary objective is to assess the strength and stiffness of materials and products under the application of crushing loads. Typically, these tests involve applying compressive pressure to the test specimen using platens or specialized fixtures with a testing machine specifically designed to generate compressive loads. The force curves showed that the wild-type group had the highest failure force, which was slightly higher than the d6OA-25 group and the mab-25 group (Figure 5A). The graph bar showed that d6OA-25 group had higher failure force (+48%; p < 0.05) over the OA-25 group. There were no significant differences in the above parameters between the d6OA group and the mab group (p > 0.05) (Figure 5B).

The binding sites in sclerostin interacting with the 5-quinoline modified aptamer were altered when compared with those interacting with unmodified aptamers

Among all the selected aptamers (including single/multiple quinoline-modified aptamers and naturally unmodified aptamer), 5-quinoline modification was predicted to possess the greatest number of interactions (totally 17 interactions) and smallest Gibbs free energy for binding (−2,329 kJ/mol) (Figures S11A, S11B, S12, and Table S8).

Among sites 124–128 in sclerostin, sites 127–128 were predicted to form one hydrogen bond with the naturally unmodified aptamer Aptscl56 (GLY127:G22, 4.45 Å), while sites 124–126 were not predicted (Figure 6A, Table S8). Interestingly, sites 124–126 were predicted to form one shorter hydrogen bond with Aptscl56-d6 (CYS124:G18, 2.27 Å), while sites 127–128 were not predicted (Figure 6B, Table S8). Compared with the predicted hydrogen bond length between site 128 in sclerostin and the naturally unmodified aptamer (Aptscl56), the predicted hydrogen bond length between sites 124–126 and Aptscl56-d6 was significantly shorter, implying a stronger intermolecular interaction for binding.

Consistently, the BLI data demonstrated that the binding ability of Aptscl56-d6 to sclerostin was abolished after mutation of site 124–126 in sclerostin, whereas the binding ability of Aptscl56-d6 to sclerostin remained unchanged after mutation of sites 127–128 in sclerostin (Figures 6C and 6D). It suggested that sites 124–126 rather than sites 127–128 in sclerostin participated in the interactions to the 5-quinoline modified aptamer. Interestingly, the binding ability of Aptscl56 to sclerostin was abolished after mutation of sites 127–128 in sclerostin, whereas the binding ability of Aptscl56 to sclerostin

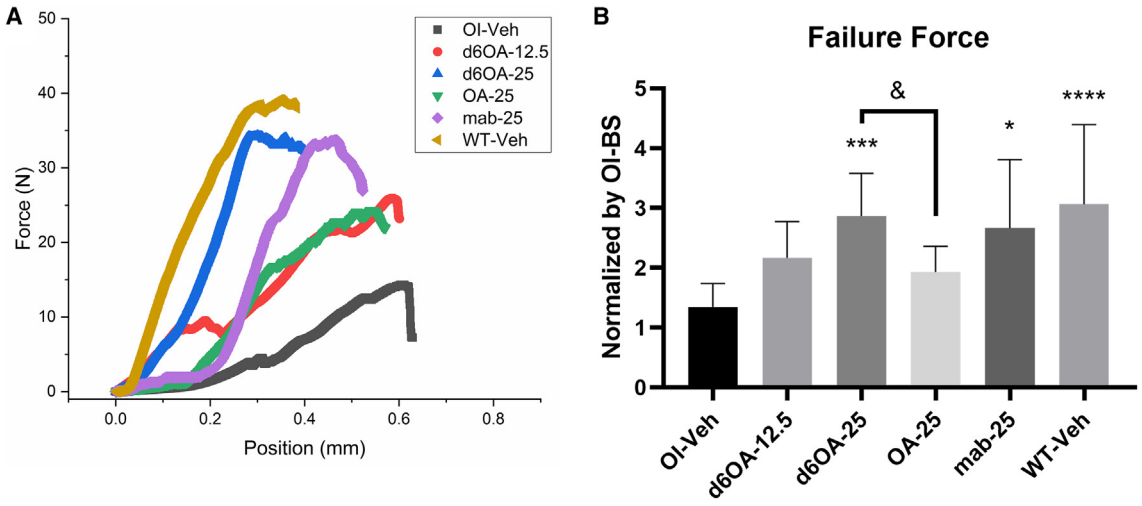

Figure 5. 5-Quinoline could facilitate the modified Aptscl56 enhancing bone mechanical properties of the Lv5 in *Col1a2*$^{+/G610c}$ OI mice

(A) Compression test for the normalized value of failure force at the Lv5. Representative curves showing the mechanical properties of the Lv5 by compression test. (B) Analysis of bone mechanical properties parameters of failure force at the Lv5. n ≥ 6 each group. Note: OI-BS, OI-Baseline; OI-Veh, OI-Vehicle; d6OA-12.5, Aptscl56-md6OA (12.5 mg/kg); d6OA-25, Aptscl56-md6OA (25 mg/kg); OA-25, Aptscl56-mOA (25 mg/kg); mab-25, sclerostin antibody (25 mg/kg); WT-Veh, WT-Vehicle. Data were expressed as mean ± SD followed by one-way ANOVA with Tukey's post-hoc test. *$p < 0.05$; ***$p < 0.001$; ****$p < 0.0001$ versus OI-Veh; $^{\&}p < 0.05$ versus OA-25.

remained unchanged after mutation of sites 124–126 in sclerostin (Figures 6C and 6D). It suggested that sites 127–128 rather than sites 124–126 in sclerostin participated in the interactions to the naturally unmodified aptamer. Together, the aptamer interacting sites in sclerostin shifted from sites 127–128 to sites 124–126 after 5-quinoline modification, indicating that 5-quinoline modification could facilitate altering the binding conformation of the modified aptamer to sclerostin.

The mutation of the newly participated binding site in sclerostin could not only reduce the binding ability of the modified aptamer to sclerostin, but also attenuate the re-activation effect of the modified aptamer on the suppressed Wnt signaling *in vitro*

To mechanistically investigate the roles of the newly participated binding sites in the binding ability with the 5-quinoline modified aptamer, point mutation at sites 124, 125, and 126 in loop3 was performed, respectively. The BLI demonstrated that the binding ability of Aptscl56-d6 to sclerostin was significantly attenuated after mutation of site 124 in sclerostin, whereas the binding ability of Aptscl56-d6 to sclerostin slightly attenuated after mutation of site 127 or site 128 in sclerostin (Figure 6E). It suggested that site 124 in sclerostin played more important roles in the interactions to the 5-quinoline modified aptamer over site 125 and site 126 in sclerostin. To investigate the roles of the site 124 in the re-activation effect of the 5-quinoline modified aptamer on the suppressed Wnt signaling, point mutation at site 124 in sclerostin (i.e., sclerostin^{C124A}) was performed. There was no significant difference in the suppressed effect on Wnt signaling of sclerostin with and without point mutation at site 124 (Figure 6F). It suggested that site 124 in sclerostin had no roles in Wnt signaling. Interestingly, the suppressed Wnt signaling by sclerostin was greatly recovered after Aptscl56-md6 treatment, whereas the suppressed Wnt signaling by sclerostin^{C124A} was hardly recovered after Aptscl56-md6 treatment (Figure 6F). It suggested that the mutation of site 124 in sclerostin attenuated the re-activation effect of the modified aptamer on the suppressed Wnt signaling *in vitro*.

DISCUSSION

Among all quinoline modifications, 5-quinoline modification remarkably facilitated enhancing the greatest binding ability of the modified aptamer to sclerostin and attenuating the suppressed effect of the transfected sclerostin on Wnt signaling *in vitro*, which could be explained by the desired conformation alteration induced by 5-quinoline modification quinoline molecule with different orientations (seven subtypes), which was predicted to tightly interact with sclerostin among all the hydrophobic moieties we considered, was incorporated into the key sites of Aptscl56 through phosphoramidite chemistry followed by solid-phase DNA synthesis. Interestingly, a more than 15-fold enhancement of binding ability could be obtained by a single 5-quinoline modification at some specific sites, which could not be achieved by the other types of quinoline modification. Further measurements demonstrated that up to 17-fold enhancement of binding affinity was achieved by a single 5-quinoline modification at site 6 (K_D value decreased from 66.8 nM to 3.9 nM). Consistently, among all the types of quinoline modification, 5-quinoline modification was predicted to possess the greatest number of interactions (totally 17 interactions) and the smallest Gibbs free energy (−2,328.732 kJ/mol). Therefore, 5-quinoline modification remarkably facilitates enhancing the greatest binding ability of the modified aptamer to sclerostin, which could be explained by the predicted largest number of interactions and smallest Gibbs free energy between 5-quinoline modified aptamer and sclerostin. Notably, it was observed that the binding energy of a single quinoline

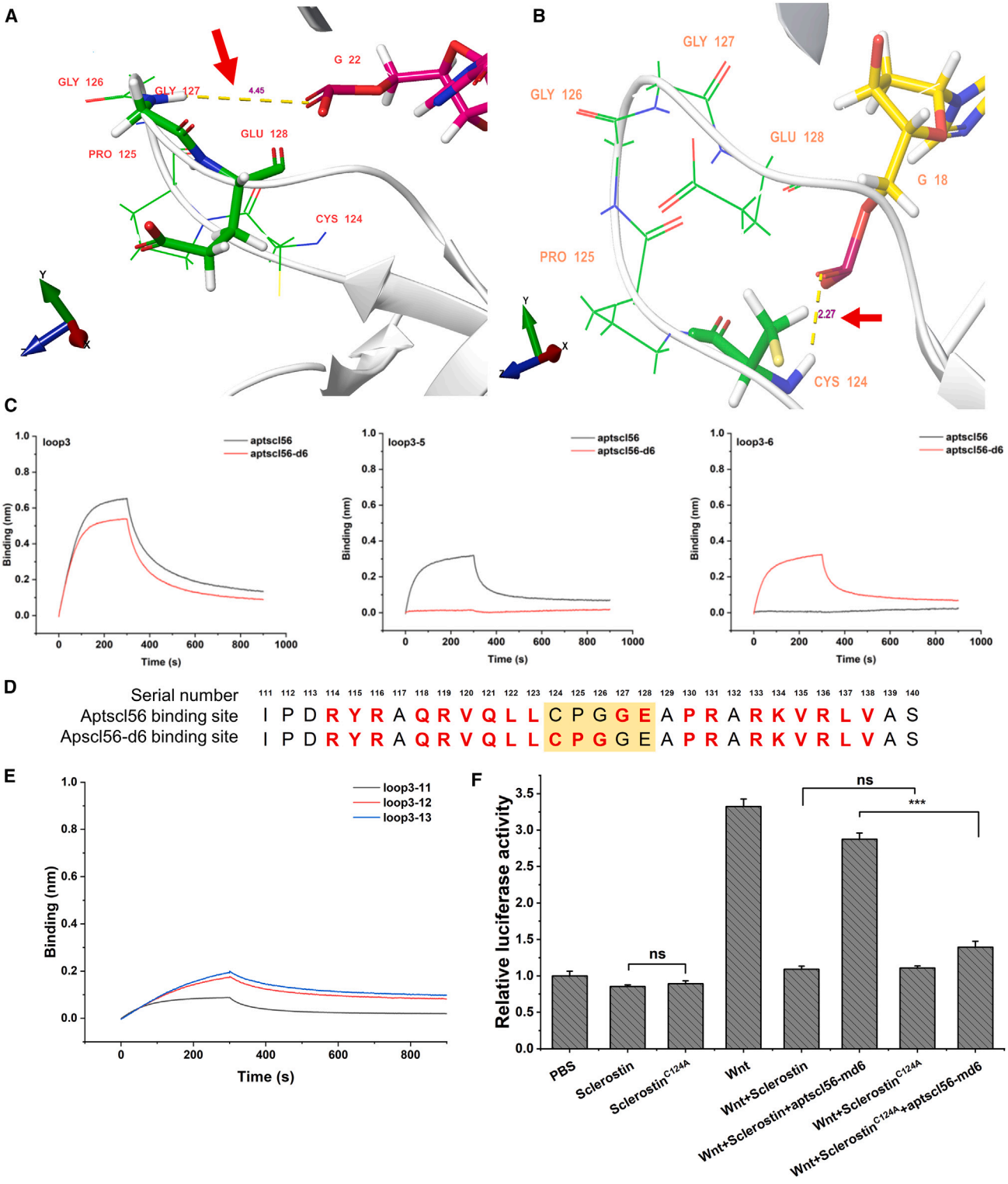

(legend on next page)

modification was lower than that of multiple modifications. Consequently, the lower K_D value of multiple quinoline-modified aptamers can be attributed to the potential influence of multiple quinoline modifications on the three-dimensional structure of the modified aptamer. This structural alteration may result in reduced interactions with the target protein. Among all the quinoline modifications, 5-quinoline modification also facilitated the modified aptamer attenuating the suppressive effect of the transfected sclerostin on Wnt signaling *in vitro* at most, which could be explained by the highest binding affinity after the 5-quinoline modification.

Structurally, the binding sites in sclerostin interacting with the 5-quinoline-modified aptamer were altered when compared with those interacting with the unmodified aptamer. Mechanistically, the mutation of the newly participated binding site (no roles in Wnt signaling) in sclerostin could not only reduce the binding ability of the modified aptamer to sclerostin, but also attenuate the re-activation effect of the modified aptamer on the suppressed Wnt signaling *in vitro*. Taken together, 5-quinoline modification could alter the conformation of the modified aptamer to sclerostin to facilitate enhancing its binding affinity and attenuating the suppressed effect of the transfected sclerostin on Wnt signaling *in vitro*.

5-Quinoline modification could facilitate the modified aptamer enhancing its bone anabolic potential *in vitro* and *in vivo*

Our *in vitro* data demonstrated that 15%–19% enhancements of mRNA expression levels (*Runx2*, *Alp*, and *Ocn*) in MC3T3-E1 cells were achieved by a single 5-quinoline modification, indicating that 5-quinoline modification could facilitate the modified aptamer enhancing mRNA expression levels of the bone formation markers *in vitro*. Consistently, 5-quinoline modification facilitated the modified aptamer promoting bone formation (+24% Tb.BFR/BS for distal femur) *in vivo*. Structurally, 5-quinoline modification could facilitate the modified aptamer increasing bone mass (+40% Tb.vBMD for distal femur and +118% Tb.vBMD for proximal tibia), improving bone microarchitecture integrity (+33% Tb.N and +49% Tb.Conn.D for distal femur; +48% Tb.Conn.D for proximal tibia; +11.3% Ct. periosteal perimeter and +38.3% Ct. bone strength index for femoral mid-shaft) and enhancing bone mechanical properties (+48% failure force for the 5th lumbar vertebrae), which could be explained by that 5-quinoline modification could facilitate the modified aptamer promoting bone formation *in vivo*. Although 5-quinoline molecule was small, the 5-quinoline-induced differences in accumulation or clearance from the system could not be excluded. The pharmacokinetics of aptamers with and without 5-quinoline modification should be investigated in the future.

5-Quinoline modification strategy could help to address the druggability bottleneck of the nucleic acid aptamers with low affinity

A more than 17-fold enhancement of binding affinity was obtained by 5-quinoline modification. Functionally, 5-quinoline modification could facilitate the modified aptamer, attenuating the suppressed effect of the transfected sclerostin on both Wnt signaling *in vitro*, which was almost the same level of that induced by the sclerostin antibody romosozumab ($p > 0.05$). Pharmacologically, 5-quinoline modification could facilitate the modified aptamer attenuating the suppressed effect of the transfected sclerostin on bone formation marker expression levels (*Runx2*, *Alp*, and *Ocn*) *in vitro*, which was also the same level of that treated with the sclerostin antibody romosozumab ($p > 0.05$). Consistently, there were no significant differences in the Tb.BFR/BS for distal femur, Tb.vBMD for both distal femur and proximal tibia, failure force for the fifth lumbar vertebrae (Lv5), Tb.N for distal femur, Tb.Conn.D for both distal femur and proximal tibia, Ct. periosteal perimeter for femoral mid-shaft, and Ct. bone strength index for femoral mid-shaft between d6OA group and mab group ($p > 0.05$). It indicated that 5-quinoline modification could facilitate the modified aptamer, increasing bone mass, improving bone microarchitecture integrity, enhancing bone mechanical properties, and promoting bone formation *in vivo*, which was almost the same level of that treated with the sclerostin antibody romosozumab. Taken together, a 5-quinoline modification strategy could help to address the druggability bottleneck of the nucleic acid aptamers with low affinity.

MATERIALS AND METHODS

Materials

The DNA aptamers used in this study were synthesized by H8 DNA/RNA synthesizer (K&A Laboratories). The common phosphoramidites, C3 spacer phosphoramidite, dspacer THF phosphoramidite, and Benzyl-amine phosphoramidite for benzyl modification were purchased from Chemvon Biotechnology CO., LTD. The other compounds

Figure 6. 5-Quinoline modification could alter the conformation of the modified aptamer to facilitate enhancing both its binding affinity to sclerostin and its re-activation effect on the suppressed Wnt signaling *in vitro*

(A) Sited 127–128 in sclerostin were predicted to form one hydrogen bond (red arrow) with naturally unmodified aptamer (Aptscl56) (GLY127:G22, 4.45 Å), whereas sited 124–126 in sclerostin were not predicted. (B) Sites 124–126 in sclerostin were predicted to form one hydrogen bond (red arrow) with 5-quinoline modified aptamer (Aptscl56-d6) (CYS124:G18, 2.27 Å), whereas sites 127–128 in sclerostin were not predicted. (C) The measured binding ability of the Aptscl56 and Aptscl56-d6 to sclerostin loop 3, loops 3–5 (mutation of sites 124–126 in sclerostin), and loops 3–6 (mutation of sites 127–128 in sclerostin), respectively, by BLI. (D) The binding sites of sclerostin loop 3 to Aptscl56 and Aptscl56-d6, respectively. The provided serial number is the amino acid sequence of sclerostin loop 3. Note: the amino acids in bold and red were those detected binding sites of loop 3 to the aptamer. The difference in the binding sites between Aptscl56 and Aptscl56-d6 was highlighted in gold. (E) The measured binding ability of Aptscl56-d6 to sclerostin loops 3–11 (mutation of site 124 in sclerostin), loops 3–12 (mutation of site 125 in sclerostin), and loops 3–13 (mutation of site 126 in sclerostin), respectively, by BLI. (F) The re-activation effect of the 5-quinoline modified aptamer on the suppressed Wnt signaling by sclerostin with and without mutation on site 124 *in vitro*. Data were normalized by parameters in the PBS groups and expressed as mean ± SD. One-way ANOVA with Tukey test was used to determine the inter-group differences, respectively. $n \geq 3$ each group. $^*p < 0.05$, $^{**}p < 0.01$, $^{***}p < 0.001$. Note: PBS represented groups treated with 1× PBS, which had the same volume with other groups. sclerostin represented groups transfected with sclerostin. sclerostin^{C124A} represented groups transfected with sclerostin mutated at site 124. Wnt, groups transfected with Wnt-1.

were purchased from Aldrich Sigma. Penicillin-Streptomycin was purchased from Gibco by Life Technology. Fetal bovine serum (FBS) and lipofectamine 2000 were purchased from Thermo Fisher Scientific. PBS was purchased from HAKATA. DMEM, MEM-α medium and OptiMem Medium were purchased from Omacgene. Serum-free cell freezing medium was purchased from Beijing T&L Biological Technology Co., Ltd. TransZol Up Plus RNA Kit was purchased from TransGen Biotech. A High-capacity cDNA Reverse Transcription Kit was purchased from Applied Biosystems. SYBR Green qPCR Mix was purchased from Magic-bio. The biotinylated DNAs and primers used in this study were purchased from Biosyntech. Passive lysis buffer (PLB) and Dual-Luciferase Reporter Assay System were purchased from Promega. The plasmids used in this study were purchased from GenScript Biotech Corporation. FinePure EndoFree Plasmid Mini Kit was purchased from Genfine Biotech (Beijing) CO., Ltd. The recombinant proteins were purchased from Abcam. The 2.0 mL microcentrifuge tubes were purchased from SORFA. The shake flask was purchased from NEST Biotechnology Co. Ltd. The TCF/LEF Luciferase Reporter HEK293 Cells were purchased from BPS Bioscience LTD. The MC3T3-E1 Cells were purchased from ATCC. The OI mice (*Col1a2*$^{+/G610C}$ mice) and wild-type mice were purchased from the Laboratory Animal Services Center in the Chinese University of Hong Kong (LASEC, CUHK). Romosozumab was purchased from Amgen.

Preparation of the compound 1a-1g and 2a-2g using carbon monoxide incorporation strategy

Compound 1a-1g

To a 100-mL high-pressure kettle, we added 1-(2′-deoxy-5′-dimethoxytrityl-β-D-ribofuranosyl)-5-iodouracil (2.0 g, 3.0 mmol), aminomethyl-quinolines (0.95 g, 6.0 mmol) respectively, and tetrakis(triphenylphosphine)palladium(0) (35 mg, Pb 10%).[10] We subsequently added 20 mL anhydrous THF to dissolve the above reactants, followed with the addition of Et_3N (2.1 mL, 15 mmol). We covered the kettle lid and turned on the carbon monoxide cylinder pressure reducing valve. We replaced the space left with carbon monoxide three times, and then filled it with carbon monoxide at a pressure of 0.30–0.40 MPa. Then the reaction kettle was placed in an oil bath at 60°C–70°C and stirred for 3–4 days. During the procedure, if the pressure in the kettle dropped below 0.30 MPa, carbon monoxide gas was used to maintain a pressure between 0.30 and 0.40 MPa.

We placed the reaction kettle in an ice water for 20 min, and then released the pressure in a fume hood. We opened the kettle and poured the reaction solution into 100 mL ice water, followed with extraction by 50 mL ethyl acetate three times. We dried the organic phase with anhydrous Na_2SO_4, and concentrated it *in vacuo*. Next, neutral silica was applied to purify final products with an eluent of n-hexane/ethyl acetate = 1/2 (one drop of Et_3N was recommended). After concentrated and evaporated to dryness, the products were obtained as viscous solids (yields: **1a**: 66%, 1b: 72%, 1c: 65%, **1d**: 12%, **1e**:60%, **1f**: 68%, **1g**: 53%) (Figures S13–S19).

Compound 2a-2g

To a solution of 3.3 mmol of **1a**-**1g** (2.4 g) in anhydrous DCM (50 mL) was added tetrazole (0.69 g, 9.8 mmol) and 2-cyanoethyl-N,N,N′,N′-tetraisopropylphosphorodiamidite (2.9 g, 9.8 mmol) with an ice-water bath under N_2 protection. Then the solution was moved to room temperature. After stirring for 2 h, the solution was concentrated *in vacuo* and the residue was then purified by flash chromatography (n-hexane/ethyl acetate = 1/1) to afford the desired product **2a**-**2g** as viscous and pale-yellow solids (yields: **2a**: 61%, 2b: 72%, **2c**: 48%, **2d**: 70%, **2e**:58%, **2f**: 79%, **2g**: 52%) (Figures S20–S26).

Preparation of modified aptamers

For small-scale synthesis of naturally unmodified aptamers and chemically modified aptamers for *in vitro* study was manipulated by H-8 DNA/RNA Oligo Synthesizer (K&A Labs). After deprotection from the solid phase, the aptamers were purified by Agilent 1260 Semi-Prep LC System, followed with characterizing by mass spectrum. Large scale synthesis of aptamers for *in vivo* study was manipulated by AKTA oligopilot 100 (Cytiva, USA). After deprotection from the solid phase, the aptamers were purified by Autotide 100 Oligo Purification System, followed with characterizing by mass spectrum. To extend the half-life of aptamers, Aptscl56-m and Aptscl56-md6 (Figure S26) were conjugated to a semaglutide side chain to afford Aptscl56-mOA (Figure S27) and Aptscl56-md6OA (Figure S28), respectively (PCT/CN2022/082996).

ELONA

We coated a 160-ng target protein to 96-well microtiter plate in 100 μL SELEX B&W buffer (1 mM $MgCl_2$ in 1× PBS containing 0.05% Tween 20) by incubating at 4°C overnight. The plate was then blocked with blocking buffer (1× PBS containing 0.1% Tween 20 and 1% BSA) for 1 h at room temperature and washed with SELEX B&W buffer four times. We then added 1 μM biotinylated aptamers into each well, added SELEX B&W buffer to 100 μL and incubated it for 45 min at room temperature with continuous gentle shaking. After binding, the plate was washed with washing buffer (1 mM $MgCl_2$ in 1× PBS containing 0.1% Tween 20 and 0.1% BSA) four times to remove non-specific and very weak binding. We added 100 μL streptavidin-HRP (1:10,000 dilute into washing buffer) to each well and incubated for 30 min and washed with washing buffer four times. We added 50 μL TMB to each well and incubated for 20 min. The reaction was stopped by adding 50 μL 2 M H_2SO_4. Absorbance at 450 nm was measured with a microplate reader.

BLI assay

The interactions between selected aptamers (100 nM) and sclerostin/loop 3/loop 3 mutates (50 nM) were analyzed using the Octet 96/96e system (ForteBio) at 25°C. Running processes and conditions were as follows: Baseline: 1× PBS buffer (10 mM phosphate buffer, 2.7 mM KCl, and 137 mM NaCl, pH 7.4), 120 s, 1,000 rpm; Loading: 100 nM 5-biotinated aptamer in 1× PBST buffer (1× PBS +0.02% Tween 20, pH 7.4), 600 s, 500 rpm; Baseline 2: 1× PBST buffer, 300 s, 500 rpm; Association: sclerostin (20 nM, 16 nM, 12 nM, 8 nM, 4 nM, 0 nM) in 1× PBST buffer, 600 s, 500 rpm; Dissociation: 1× PBST buffer, 600 s,

500 rpm; Regeneration: 5 M NaCl, 30 s, 500 rpm; and Neutralization: 1× PBS buffer, 60 s, 500 rpm. Finally, the affinity constant K_D values were calculated by fitting curves into a 1:1 binding model with ForteBio Data analysis 11.0.

Serum stability

The DNA aptamers (0.4 μM) were incubated in 10% FBS solution (30 μ) at a temperature 37°C. After a time point (0 min, 1 h, 2 h, 4 h, 8 h, 16 h, and 32 h), 4 μL of the mixtures was collected, followed by addition of DNA loading buffer and formamide (deionized). Next, the resulting samples were electrophoresed on 20% denaturing urea polyacrylamide gel at 220 V for 40 min. After that, the gels were photographed by usage of ChemiDoc XRS System (BioRad), and analyzed in Image Lab software.

Site-directed mutagenesis

The pLVX-IRES-ZsGreen1-sclerostin was used as the template. The codons in the target sites C124 were replaced with the codon encoding alanine (GCC) by whole-plasmid PCR (forward primer: CGCGTG CAGCTGCTGGCCCCCGGTGGTGAGGCG; reverse primer: CGC CTCACCACCGGGGGCCAGCAGCTGCACGCG). The amplified PCR products were digested by *Dpn*I for 2.5 h to remove the template plasmids before conversion into *E. coli* DH5α-competent cells. Colonies carrying recombinant plasmid were picked up to cultivate for 10–12 h after verification by colony PCR and restriction enzyme digestion. After gene sequencing, the recombinant strains were cultivated in 100-mL shaking flask for 20–24 h to obtain enough cells for plasmid extraction. Subsequently, the plasmid extraction was manipulated under the instruction of FinePure EndoFree Plasmid Mini Kit.

Evaluating the effect of the 5-quinoline-modified aptamer on the suppressed Wnt signaling induced by the transfected sclerostin/sclerostin^{C124A}

Referring to a published protocol,[21,22] the TCF/LEF luciferase Reporter HEK293 cells were cultured at 37°C under humidified atmosphere and 5% CO_2 with DMEM containing 10% FBS and 1% penicillin-streptomycin (Gibco by Life Technology). After seeded on 96-well plate at a density of 5×10^4 in 100 μL DMEM, the cells were cultured 24 h. A Wnt-1 plasmid (25 ng/well) and a sclerostin/sclerostin^{C124A} plasmid (25 ng/well) were co-transfected into the cells using lipofectamine 2000 (0.35 μL per well). During the process, the plasmids and lipofectamine 2000 were first mixed in 30 μL OptiMem medium and incubated for 20 min. Then, 70 μL DMEM without serum and antibiotic was added and mixed slightly. Finally, the transfection mixture was moved to the cells upon the removing of the old medium. After 12 h, the transfection mixture was removed and 100 μL normal growth medium containing either 500 nM romosozumab or 500 nM aptamer was added. After incubating at 37°C for 12 h, the medium was removed and the cells were lysed in 100 μL 1× PLB by shaking the culture vessel for 15 min at room temperature. Then, 15 μL lysate was transferred to 96-well OptiPlate to determine the luciferase activity by measuring the chemiluminescence using SpectraMax i3X Multi-Mode Microplate Reader (Molecular Devices) under the manufacturing protocol of Dual-Luciferase Reporter Assay System.

The EC_{50} measurement of aptamers against sclerostin *in vitro*

The TCF/LEF luciferase Reporter HEK293 cells were seeded on 96-well plate at a density of 5×10^4 in 100 μL DMEM. After the cells were cultured for 24 h, the Wnt-1 plasmid (25 ng/well) and the sclerostin plasmid (25 ng/well) were co-transfected into the cells using lipofectamine 2000 (0.35 μL/well). After 12 h, the transfection mixture was removed and 100 μL normal growth medium containing different concentration of Aptscl56 or Aptscl56-md6 (0, 5, 10, 20, 40, 80, 160, 320, and 640 nM, respectively) was added. After incubating at 37°C for 12 h, the medium was removed and the cells were lysed in 100 μL 1× PLB by shaking the culture vessel for 15 min at room temperature. Then, 15 μL lysate was transferred to 96-well OptiPlate to determine the luciferase activity by measuring the chemiluminescence using SpectraMax i3X Multi-Mode Microplate Reader system under the manufacturing protocol of Dual-Luciferase Reporter Assay System. Finally, the data were analyzed by Origin 2019b (Description: Nonlinear Curve Fit, Iteration Algorithm: Levenberg Marquuardt, Model: DoseResp).

Real-time qPCR

MC3T3-E1 (mouse preosteoblast, ATCC CRL-2593) cell line was cultured in MEM-α medium supplemented with 10% FBS and 100 units/mL penicillin-streptomycin. After seeded in 24-well plates with a density of 2×10^5 cells/well, the cells were cultured for 24 h the Wnt-1 plasmid (250 ng/well) and the sclerostin plasmid (250 ng/well) were co-transfected into the cells using lipofectamine 2000 (2 μL/well). During the process, the plasmids and lipofectamine 2000 were first mixed in 100 μL OptiMem medium (Omacgene) and incubated for 20 min. Then, 400 μL MEM-α without serum and antibiotic was added and mixed slightly. Finally, the transfection mixture was moved to the cells upon the removing of the old medium. After 6 h, the transfection mixture was removed and 500 μL normal growth medium containing 10 mM LiCl. At the same time, either 500 nM romosozumab or 500 nM aptamer was added. After incubating at 37°C for 12 h, the medium was removed and total RNA from cultured cells was isolated by homogenization using TransZol Up Plus RNA Kit (TransGen Biotech) according to the manufacturer's instructions. After purification, the total RNA was quantified using Nanodrop 2000 (Thermo Fisher Scientific) and reversely transcribed into cDNA using a high-capacity cDNA reverse transcription kit. The primers, including *Runx2* (forward primer: CCTGAACTCTGCACCAAGTCCT; reverse primer: TCATC TGGCTCAGATAGGAGGG),[23] *Alp* (forward primer: CCAGAAA GACACCTTGACTGTGG; reverse primer: TCTTGTCCGTGTCGC TCACCAT),[23] and *Ocn* (forward primer: GCAATAAGGTAGTGA ACAGACTCC; reverse primer: CCATAGATGCGTTTGTAGGC GG),[24] *Gapdh* (forward primer: CATCACTGCCACCCAGAAG ACTG; reverse primer: ATGCCAGTGAGCTTCCCGTTCAG).[25] Quantitative PCR reactions were performed using the SYBR Green qPCR Mix on the 7900 HT Sequence Detection System (Applied Biosystems). Relative RNA expression of gene was determined using the $2^{-\Delta\Delta Ct}$ method by using *Gapdh* as the endogenous normalizer.

Bone histomorphometric analysis

The procedures of all animal studies have obtained ethics approval by the Animal Experimentation Ethics Committee of the Hong Kong

Baptist University (REC/22–23/0121). All experiments conform to all relevant regulatory standards. All the animals were injected intraperitoneally with 50 μL calcein (20 mg/kg) at the 13th and the 3rd days before euthanasia, respectively. After sacrificing, the bone tissues (the left femurs and the left tibias) were collected and fixed in 4% Paraformaldehyde for 48 h, dehydrated in an increased 10%, 20%, and 30% concentrations of sucrose (dilution in 1× PBS) for 24 h in each concentration and embedded without decalcification in an optimal cutting temperature compound (Sakura Finetek, Co. Ltd.). After embedding, the distal femurs and proximal tibias of the samples was sectioned longitudinally, and the histomorphometric analyses of trabecular bone were performed at the above two sites. The frozen tissue specimens will be obtained at a thickness of 5 μm with CryoStar NX50 (Thermo Fisher ScientificA) and it was consistent with the selected sites of micro-CT. Fluorescence micrographs for the calcein in the bone sections were captured by a Q500MC fluorescence microscope (Leica). The parameters of bone dynamic histomorphometric analysis for trabecular bone included the BFR/BS and mineral apposition rate. The analysis was performed using professional histomorphometric analysis system (BIOQUANT OSTEO), and the parameters were calculated and expressed according to the American Society for Bone and Mineral Research-standardized nomenclature for bone histomorphometry.[26]

Micro-CT analysis

Cortical microarchitecture at the left femoral mid-shaft, bone mass, and trabecular microarchitecture analysis of the trabecular bone at the left proximal tibia metaphysis and the left distal femoral metaphysis, were performed with micro-CT (version 6.5, vivaCT40, SCANCO Medical AG). Images of the femur and tibia were reconstructed and calibrated at the isotropic voxel size of 12.5 and 17.5 μm, respectively (70 kVp, 114 μA, 200-ms integration time, 260 thresholds, 1,200 mg HA/cm^3). Every measurement will use the same filtering and segmentation values. Using the Scanco evaluation software, regions of interest (ROIs) will be defined for trabecular parameters. For the trabecular bone, a central region will be selected equivalent to 70% of the vertebral body height and extended from proximally to the end of the distal growth plate toward the vertebral body. For the proximal tibia and distal femur of mice, 100 sequential slices beginning at 0.1 mm from the most proximal aspect of the growth plate in which both condyles were no longer visible were selected for analysis. We drew freehand the trabeculae ROI on 100 sequential slices to ensure it will be within the endosteal envelope. Trabecular bone parameters, including Tb.vBMD, Tb.N, and Tb.conn.D were calculated. For femoral mid-shaft, 100 sequential slices were measured at the exact center and at the distal 50% of femur length using the automated thresholding algorithm. Trabeculae in contact with cortical bone were manually removed from the ROI. Cortical bone parameters, including Ct. periosteal perimeter, Ct. endosteal perimeter and Ct. bone strength index were calculated.

Bone mechanical test

The Lv5 were used to describe the bone mechanical properties through the compression test by using a universal testing machine (H25KS Series, Hounsfield Test Equipment Ltd) with a 2.5-kN load cell.[27] The Lv5s were isolated from vertebral columns and constructed into a cylinder with two parallel planes (5–7 cm) before the test. The Lv5s were positioned horizontally to the base. Load was applied constantly with displacement rate of 1 mm/min. After failure, the load vs. displacement curves were recorded, the failure force (N) and ultimate strength (MPa) were calculated for statistical analysis.

Aptamer structural modeling and molecular docking

The secondary structure of the unmodified aptamer was predicted using RNAfold (http://rna.tbi.univie.ac.at//cgi-bin/RNAWebSuite/RNAfold.cgi) and the three-dimensional structure was predicted using RNAcomposer (https://rnacomposer.cs.put.poznan.pl/). Resulting model with the lowest Gibbs free energy was imported into Molecular Operating Environment (MOE) software and all the hydroxyls at the 2′-position of all sugars were manually removed to obtain the exact unmodified DNA aptamer structure (Aptscl56). Energy minimization was conducted to obtain the final PDB file which was further used for docking.[6–8] For 5-quinoline modified aptamer, the 5-quinoline moiety was connected manually to the 6-site of unmodified aptamer and energy minimization was also performed within MOE software. Molecular docking experiments were performed using Schrödinger software suite. The receptor (PDB ID: 2K8P) and the above aptamer files considered as protein files were imported and optimized using Protein Preparation Workflow Pane in Maestro. Protein-Protein Docking Pane was performed and sclerostin loop 3 (site 111–145) was used to generate a grid for docking, and Prime protein structure prediction program as well as standard Glide settings were performed for docking.[9,10] The generated poses and potential interactions were analyzed in Maestro and Pymol.

Small molecule docking

The three-dimensional structures of hydrophobic candidates were generated using Chem3D. Energy minimization was conducted to obtain the final mol2 file which was further used for docking. Molecular docking experiments were performed using Schrödinger software suite. The receptor (PDB ID: 2K8P) and the above hydrophobic candidate files were imported and optimized using Glide Ligand Docking Pane. The generated poses and potential interactions were analyzed in Maestro and Pymol.

Statistical analysis

All variables were expressed as mean ± SD. A paired t test was used to determine the differences between mutants and naturally unmodified Aptscl56 in the identification of key sites in the aptamer interacting with sclerostin. One-way ANOVA with Tukey's post-hoc test was performed to determine the inter-group differences in the study variables, including for *in vitro* Wnt induced signaling, *in vitro* mRNA levels of bone formation biomarkers, micro-CT parameters, bone histomorphometric parameters, and mechanical test. All the statistical data were analyzed by Origin 2019b and GraphPad Prism, and a p value of less than 0.05 was considered to be statistically significant. For the *in vivo* experiments, the animals were grouped randomLy and

blindly to researchers. The animals in poor body condition were excluded.

DATA AND CODE AVAILABILITY

The authors declare that the data supporting the findings of this study are available within the paper and its supplementary information files. Source data are provided with this paper.

SUPPLEMENTAL INFORMATION

Supplemental information can be found online at https://doi.org/10.1016/j.omtn.2024.102146.

ACKNOWLEDGMENTS

This study was supported by the Young Scientists Fund of the National Natural Science Foundation of China (82304378), the Guangdong Basic and Applied Basic Research Foundation (2020A15 15110630), Guangdong-Hong Kong Technology Cooperation Funding Scheme (GHP/149/21GD, 2023A0505010015), National Key R&D Program of China (2018YFA0800802), CUHK Direct Grant (4054714), Theme-based Research Scheme (T12-201-20R), Interdisciplinary Research Clusters Matching Scheme of Hong Kong Baptist University (RC-IRCs/17-18/02), Key-Area R&D Program of Department of Science and Technology of Hunan Province (2022WK2010), and Science, Technology and Innovation Commission of Shenzhen Municipality Funds (JCYJ20160229210357960).

AUTHOR CONTRIBUTIONS

A.G. and Y.M. wrote the manuscript with the input from all authors; A.G., Y.M., S.Y., H.Z., and Z.C. designed and performed the *in vitro* and *in vivo* study; S.N. and A.G. helped in the synthesis of small molecules and modified aptamers; H.X., Y.Z., H.D., and H.L. performed the computational work; Y.Y. and L.W. designed the mutated sclerostin loop3; H.J. and N.J. designed the mutated sclerostin plasmid; Y.T. and H.L. assisted with bone samples processing; S.N. and A.L. helped revising the manuscript and proposed constructive discussions; Y.M., B.Z., and G.Z. devised the project and supervised the preparation of the manuscript.

DECLARATION OF INTERESTS

The authors declare that the research was conducted in the absence of any commercial or financial relationships that could be construed as a potential conflict of interest.

REFERENCES

1. Shraim, A.S., Abdel Majeed, B.A., Al-Binni, M.A., and Hunaiti, A. (2022). Therapeutic Potential of Aptamer-Protein Interactions. ACS Pharmacol. Transl. Sci. *5*, 1211–1227. https://doi.org/10.1021/acsptsci.2c00156.

2. Qi, S., Duan, N., Khan, I.M., Dong, X., Zhang, Y., Wu, S., and Wang, Z. (2022). Strategies to manipulate the performance of aptamers in SELEX, post-SELEX and microenvironment. Biotechnol. Adv. *55*, 107902. https://doi.org/10.1016/j.biotechadv.2021.107902.

3. Dong, H.Y., Xie, Q.H., Pang, D.W., Chen, G., and Zhang, Z.L. (2021). Precise selection of aptamers targeting PD-L1 positive small extracellular vesicles on magnetic chips. Chem. Commun. *57*, 3555–3558. https://doi.org/10.1039/d1cc00168j.

4. Sarkar, A., Jayesh Sodha, S., Junnuthula, V., Kolimi, P., and Dyawanapelly, S. (2022). Novel and investigational therapies for wet and dry age-related macular degeneration. Drug Discov. Today *27*, 2322–2332. https://doi.org/10.1016/j.drudis.2022.04.013.

5. Kumar Kulabhusan, P., Hussain, B., and Yüce, M. (2020). Current Perspectives on Aptamers as Diagnostic Tools and Therapeutic Agents. Pharmaceutics *12*, 646. https://doi.org/10.3390/pharmaceutics12070646.

6. Fan, X., Sun, L., Li, K., Yang, X., Cai, B., Zhang, Y., Zhu, Y., Ma, Y., Guan, Z., Wu, Y., et al. (2017). The bioactivity of D-/L-isonucleoside- and 2'-deoxyinosine-incorporated aptamer AS1411s including DNA replication/microRNA expression. Molecular therapy. Nucleic acids *9*, 218–229. https://doi.org/10.1016/j.omtn.2017.09.010.

7. Mann, A.P., Somasunderam, A., Nieves-Alicea, R., Li, X., Hu, A., Sood, A.K., Ferrari, M., Gorenstein, D.G., and Tanaka, T. (2010). Identification of thioaptamer ligand against E-selectin: potential application for inflamed vasculature targeting. PLoS One *5*, e13050. https://doi.org/10.1371/journal.pone.0013050.

8. Cai, S., Yan, J., Xiong, H., Liu, Y., Peng, D., and Liu, Z. (2018). Investigations on the interface of nucleic acid aptamers and binding targets. Analyst *143*, 5317–5338. https://doi.org/10.1039/c8an01467a.

9. Hasegawa, H., Savory, N., Abe, K., and Ikebukuro, K. (2016). Methods for Improving Aptamer Binding Affinity. Molecules *21*, 421. https://doi.org/10.3390/molecules21040421.

10. Davies, D.R., Gelinas, A.D., Zhang, C., Rohloff, J.C., Carter, J.D., O'Connell, D., Waugh, S.M., Wolk, S.K., Mayfield, W.S., Burgin, A.B., et al. (2012). Unique motifs and hydrophobic interactions shape the binding of modified DNA ligands to protein targets. Proc. Natl. Acad. Sci. USA *109*, 19971–19976. https://doi.org/10.1073/pnas.1213933109.

11. Gawande, B.N., Rohloff, J.C., Carter, J.D., von Carlowitz, I., Zhang, C., Schneider, D.J., and Janjic, N. (2017). Selection of DNA aptamers with two modified bases. Proc. Natl. Acad. Sci. USA *114*, 2898–2903. https://doi.org/10.1073/pnas.1615475114.

12. Wu, D., Katilius, E., Olivas, E., Dumont Milutinovic, M., and Walt, D.R. (2016). Incorporation of Slow Off-Rate Modified Aptamers Reagents in Single Molecule Array Assays for Cytokine Detection with Ultrahigh Sensitivity. Anal. Chem. *88*, 8385–8389. https://doi.org/10.1021/acs.analchem.6b02451.

13. Smirnov, I., Kolganova, N., Troisi, R., Sica, F., and Timofeev, E. (2021). Expanding the recognition interface of the thrombin-binding aptamer HD1 through modification of residues T3 and T12. Mol. Ther. Nucleic Acids *23*, 863–871. https://doi.org/10.1016/j.omtn.2021.01.004.

14. Marini, J.C., Forlino, A., Bächinger, H.P., Bishop, N.J., Byers, P.H., Paepe, A.D., Fassier, F., Fratzl-Zelman, N., Kozloff, K.M., Krakow, D., et al. (2017). Osteogenesis imperfecta. Nat. Rev. Dis. Prim. *3*, 17052. https://doi.org/10.1038/nrdp.2017.52.

15. Jacobsen, C.M., Barber, L.A., Ayturk, U.M., Roberts, H.J., Deal, L.E., Schwartz, M.A., Weis, M., Eyre, D., Zurakowski, D., Robling, A.G., and Warman, M.L. (2014). Targeting the LRP5 pathway improves bone properties in a mouse model of osteogenesis imperfecta. J. Bone Miner. Res. *29*, 2297–2306. https://doi.org/10.1002/jbmr.2198.

16. Saag, K.G., Petersen, J., Brandi, M.L., Karaplis, A.C., Lorentzon, M., Thomas, T., Maddox, J., Fan, M., Meisner, P.D., and Grauer, A. (2017). Romosozumab or Alendronate for Fracture Prevention in Women with Osteoporosis. N. Engl. J. Med. *377*, 1417–1427. https://doi.org/10.1056/NEJMoa1708322.

17. Wang, L., Yu, Y., Ni, S., Li, D., Liu, J., Xie, D., Chu, H.Y., Ren, Q., Zhong, C., Zhang, N., et al. (2022). Therapeutic aptamer targeting sclerostin loop3 for promoting bone formation without increasing cardiovascular risk in osteogenesis imperfecta mice. Theranostics *12*, 5645–5674. https://doi.org/10.7150/thno.63177.

18. Yu, Y., Wang, L., Ni, S., Li, D., Liu, J., Chu, H.Y., Zhang, N., Sun, M., Li, N., Ren, Q., et al. (2022). Targeting loop3 of sclerostin preserves its cardiovascular protective action and promotes bone formation. Nat. Commun. *13*, 4241. https://doi.org/10.1038/s41467-022-31997-8.

19. Nimjee, S.M., White, R.R., Becker, R.C., and Sullenger, B.A. (2017). Aptamers as Therapeutics. Annu. Rev. Pharmacol. Toxicol. *57*, 61–79.

20. Hirao, I., Kimoto, M., and Lee, K.H. (2018). DNA aptamer generation by ExSELEX using genetic Alphabet expansion with a mini-hairpin DNA stabilization method. Biochimie *145*, 15–21. https://doi.org/10.1016/j.biochi.2017.09.007.

21. Moreno, S.E., Massee, M., Bara, H., and Koob, T.J. (2021). Dehydrated human amniotic membrane modulates canonical Wnt signaling in multiple cell types in vitro. Eur. J. Cell Biol. *100*, 151168. https://doi.org/10.1016/j.ejcb.2021.151168.

22. Nathubhai, A., Haikarainen, T., Koivunen, J., Murthy, S., Koumanov, F., Lloyd, M.D., Holman, G.D., Pihlajaniemi, T., Tosh, D., Lehtiö, L., and Threadgill, M.D. (2017). Highly Potent and Isoform Selective Dual Site Binding Tankyrase/Wnt Signaling Inhibitors That Increase Cellular Glucose Uptake and Have Antiproliferative Activity. J. Med. Chem. *60*, 814–820. https://doi.org/10.1021/acs.jmedchem.6b01574.

23. Shahrezaee, M., Salehi, M., Keshtkari, S., Oryan, A., Kamali, A., and Shekarchi, B. (2018). In vitro and in vivo investigation of PLA/PCL scaffold coated with metformin-loaded gelatin nanocarriers in regeneration of critical-sized bone defects. Nanomedicine. *14*, 2061–2073. https://doi.org/10.1016/j.nano.2018.06.007.

24. Sugatani, T., Agapova, O., Malluche, H.H., and Hruska, K.A. (2015). SIRT6 deficiency culminates in low-turnover osteopenia. Bone *81*, 168–177. https://doi.org/10.1016/j.bone.2015.07.018.

25. Koblan, L.W., Erdos, M.R., Wilson, C., Cabral, W.A., Levy, J.M., Xiong, Z.-M., Tavarez, U.L., Davison, L.M., Gete, Y.G., Mao, X., et al. (2021). In vivo base editing rescues Hutchinson–Gilford progeria syndrome in mice. Nature *589*, 608–614. https://doi.org/10.1038/s41586-020-03086-7.

26. Li, D., Liu, J., Guo, B., Liang, C., Dang, L., Lu, C., He, X., Cheung, H.Y.-S., Xu, L., Lu, C., et al. (2016). Osteoclast-derived exosomal miR-214-3p inhibits osteoblastic bone formation. Nat. Commun. *7*, 10872. https://doi.org/10.1038/ncomms10872.

27. Lin, S., Huang, J., Fu, Z., Liang, Y., Wu, H., Xu, L., Sun, Y., Lee, W.Y.W., Wu, T., Qin, L., et al. (2015). The effects of atorvastatin on the prevention of osteoporosis and dyslipidemia in the high-fat-fed ovariectomized rats. Calcif. Tissue Int. *96*, 541–551. https://doi.org/10.1007/s00223-015-9975-7.